Appl. Phys. A 88, 647–652 (2007)
DOI: 10.1007/s00339-007-4020-y

Applied Physics A
Materials Science & Processing

B.K. MONEY
K. HARIHARAN✉

Lithium ion conduction in lithium metaphosphate based systems

Solid State Ionics Laboratory, Department of Physics, Indian Institute of Technology Madras, Chennai 600036, India

Received: 11 September 2006/Accepted: 17 March 2007
Published online: 23 May 2007 • © Springer-Verlag 2007

ABSTRACT A comparative investigation on Li^+ ion transport has been carried out in various phases of lithium metaphosphate such as (i) crystalline $LiPO_3$, (ii) glassy form as mol % $50Li_2O$-$50P_2O_5$, synthesized by melt-quenching process, (iii) single phase glass-ceramic $LiPO_3$ obtained through controlled heat treatment of mol % $50Li_2O$-$50P_2O_5$ and (iv) newly identified polymer-metal salt complex $(PEO)_6$: $LiPO_3$. All of the above materials have been characterized through XRD, DSC, optical microscopy and impedance spectroscopy techniques. The Li^+ ions, migrating with an activation energy value of 1.4 eV through "interstitial mechanism" in polycrystalline $LiPO_3$, exhibited a dc conductivity value of 2.5×10^{-8} Scm^{-1} at 280 °C. The above conductivity value was enhanced by four orders of magnitude in Li_2O-P_2O_5 glass, with an activation energy value of 0.72 eV. The glass subjected to controlled heat treatment devitrified into single phase glass-ceramic, as revealed by XRD and optical microscopy studies. The glass-ceramic exhibited better conduction characteristics compared to polycrystalline $LiPO_3$. Polycrystalline $LiPO_3$, complexed with polymer PEO has exhibited a conductivity value of 3.1×10^{-7} Scm^{-1} at 78 °C with activation energies of 0.21 and 0.88 eV for Li^+ ion migration above and below the softening point of the polymer, respectively.

PACS 66.10.Ed; 71.55.Jv; 81.30.Hd; 82.45.Gj; 82.45.Wx

1 Introduction

In recent years, accelerating interest in the ion dynamics of fast ion conductors has made it possible to interpret trends in ionic conductivity and its dependence on microstructure. Although simulation and modeling of ionic conduction [1–4] gave an idea of conduction mechanism, not many reports seem to be available concerning the actual mechanism of ionic transport with regard to the possible existence of conduction pathways. A basic model of ion transport used to describe conduction in different classes of solid electrolytes is based on the isolated hopping of the mobile ions. These mobile ions are also influenced by immobile ions of the solid lattice. It is likely that in solid electrolytes such ion–ion interaction and co-operative ion movements are important and must be taken into account if a quantitative description of ionic conductivity is to be attained. In this paper, the emphasis is placed on presenting the basic elements of ion transport and comparing the ionic conductivity in various phases of solid electrolytes possessing different gross structural features.

The investigated material, lithium metaphosphate $LiPO_3$, is unique in the sense that it exists in both the crystalline ($LiPO_3$) and the glassy phase (Li_2O- P_2O_5). This presented us with an opportunity to compare Li^+ ion mobility in ordered crystalline frameworks, disordered glassy networks and glass-ceramic ($LiPO_3$) forms, which are micro-structurally different from the crystalline and glassy phases. Additionally, we evaluated Li^+ ion mobility in a novel complex of polycrystalline $LiPO_3$ in a poly(ethylene oxide) (PEO) host matrix. The structural and dynamical aspects of PEO, as the host polymer, have been well studied and understood [5]. Ether oxygens of PEO have sufficient electron donor power, forming coordinate bonds with cations. In addition, it permits multiple intrapolymer–ion bonding with low barriers to rotation for atoms in the main chain, ensuring high flexibility and thereby, facilitating segmental motion [6–8]. Hence, poly(ethylene oxide) has been chosen as a host polymer for incorporating polycrystalline $LiPO_3$ in the present study. The purpose of the present work is to understand the mechanism of Li^+ ion transport in different phases namely polycrystalline, glass, glass-ceramic and polymer electrolyte.

2 Experimental

2.1 *Sample preparation*

Polycrystalline lithium metaphosphate ($LiPO_3$) was prepared by mixing appropriate amounts of reagent-grade lithium carbonate (Li_2CO_3) and ammonium dihydrogen phosphate ($NH_4H_2PO_4$) with a mortar and pestle. The mixture was heated in a platinum crucible at 300 °C for 4 h to get rid of NH_3, H_2O and CO_2 and then the sample was kept at 560 °C for 48 h.

To prepare mol % $50Li_2O$-$50P_2O_5$ glass, the mixture was taken in a platinum crucible and melted at about 950 °C for approximately 1 h. The mixture was occasionally stirred in order to obtain a homogeneous melt. The clear, bubble-free melted

✉ Fax: +91-44-22574852, E-mail: haran@iitm.ac.in

mixture was poured on a preheated copper plate to avoid shattering of the quenched sample and pressed by another preheated copper plate. Thus, colorless, transparent mol % $50Li_2O$-$50P_2O_5$ glass was obtained.

When mol % $50Li_2O$-$50P_2O_5$ glass was subjected to controlled heat treatment by annealing in the range between its glass transition temperature ($T_g = 323$ °C) and crystallization temperature ($T_c = 486$ °C), devitrification of the glass takes place, forming glass-ceramic.

The preparation of polymer-metal salt complex has been carried out using the solution casting method. PEO (poly ethylene oxide) (Aldrich, $M_w\ 3 \times 10^6$) and crystalline $LiPO_3$ obtained by the method described earlier were used for the preparation of the complex. Among the several weight ratios between PEO and $LiPO_3$ considered, a homogenous and stable film is formed for O/Li ratio equal to 6. Hence, the quantities of PEO and $LiPO_3$ were calculated such that for every lithium ion there are 6 ether-oxygen of the polymer. The above constituents have been dissolved in acetonitrile as the common solvent and stirred for about 24 h using a magnetic stirrer in order to obtain a homogeneous mixture. The resulting homogeneous viscous solution was poured into a clean PTFE (poly tetra fluoro ethylene) petri dish and kept in a vacuum oven maintained at 50 °C to remove all traces of solvent present in the casted solution. After approximately 48 h the thoroughly dried, freestanding polymer electrolyte film with a thickness of about 150 μm was obtained and preserved in a dessicator for further characterization.

2.2 *Measurement techniques*

The micro structural, thermal, electrical conductivity and morphological properties of the samples were analyzed using the following techniques:

X-ray diffraction: The XRD measurement was carried out using Cu K_α radiation ($\lambda = 1.5418$ Å) in a diffractometer (PANalytical X'Pert PRO). Continuous XRD patterns were recorded by measuring 2θ from 10° to 70°, with a step size of 0.01° and a scan step time of 5 s.

Differential scanning calorimetry (DSC): To analyze the thermo dynamical parameters such as glass transition temperature (T_g), crystallization temperature (T_c) and melting temperature (T_m), the calorimeter DSC 200 PC-Phox (NETZSCH) was used. Measurements were carried out at the heating rate of 10 K/min with samples (few mg) encapsulated in aluminum pans in dry N_2 atmosphere. As phase transformations occurred within narrow temperature range, the DSC plots were helpful in interpreting the sequence of transformations.

Impedance spectroscopy: The ac conductivity measurement as a function of temperature has been performed using the Keithley 3330 Impedance Analyzer in the frequency range 40 Hz to 100 KHz. The conductivity set-up used for measurement is made of quartz, with a provision for evacuation/purging inert gas. The sample holder is also made of quartz and the electrical connections are made using insulated copper wires attached to a pair of silver discs. The studied sample is placed between two silver electrodes and electrical connections are prepared using insulated copper wires. A spring load is provided to rigidly hold the sample. The temperature of the sample is measured using a chromel–alumel thermocouple with an accuracy of ± 1 °C.

Optical microscopy: The morphology of the samples was investigated using a Zeiss optical microscope (AXIOSKOP 2) with a magnification power of 20X.

3 Results and discussion

The XRD patterns of polycrystalline $LiPO_3$, glass-ceramic $LiPO_3$, polymer-metal salt complex $(PEO)_6$: $LiPO_3$ and mol % $50Li_2O$-$50P_2O_5$ glass have been displayed in Fig. 1. X-ray diffractogram of polycrystalline $LiPO_3$ exhibits four prominent peaks at angles corresponding to $2\theta = 16.3°$, 18.7°, 24.9°, and 27.4°. The calculated values of interplanar distance 'd' are in agreement with standard JCPDS values, thus confirming the formation of crystalline $LiPO_3$. The calculated unit cell parameters, namely $a = 16.45$ Å, $b = 5.405$ Å, $c = 13.806$ Å and $\beta = 98.99°$ conform to the reported monoclinic structure of $LiPO_3$ [9]. Knowing the values of a, b, c, β and the interplanar distance d, the prominent peaks have been indexed using the relation

$$1/d^2 = 1/\sin^2\beta(h^2/a^2 + k^2\sin^2\beta/b^2 + d^2/c^2 - 2hl\cos\beta/ac)\,. \quad (1)$$

The glassy nature of mol % $50Li_2O$-$50P_2O_5$ has been confirmed by XRD which shows the hallow feature at lower angles. The absence of Bragg peaks indicates the long-range disorderness in the glass.

The single-phase glass-ceramic product has also been identified through XRD as $LiPO_3$, as all the prominent peaks lie on the same 2θ values. However, the intensity of the peaks

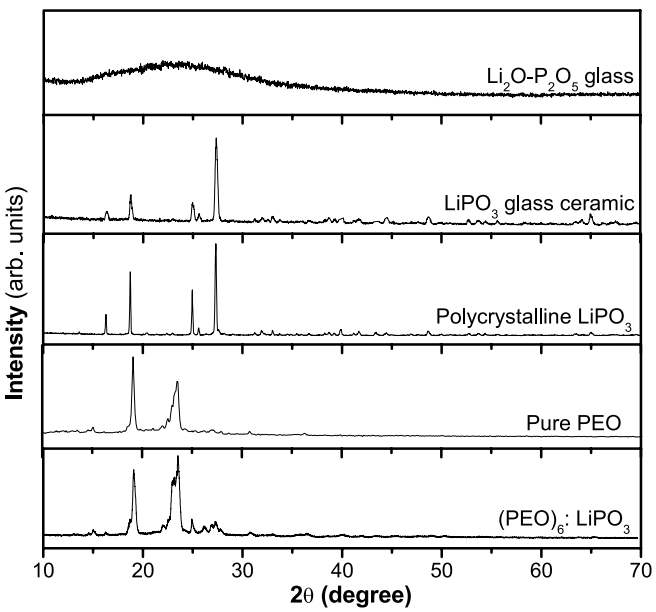

FIGURE 1 XRD of Li_2O-P_2O_5 glass, $LiPO_3$ glass-ceramic, polycrystalline $LiPO_3$, PEO and $(PEO)_6$: $LiPO_3$

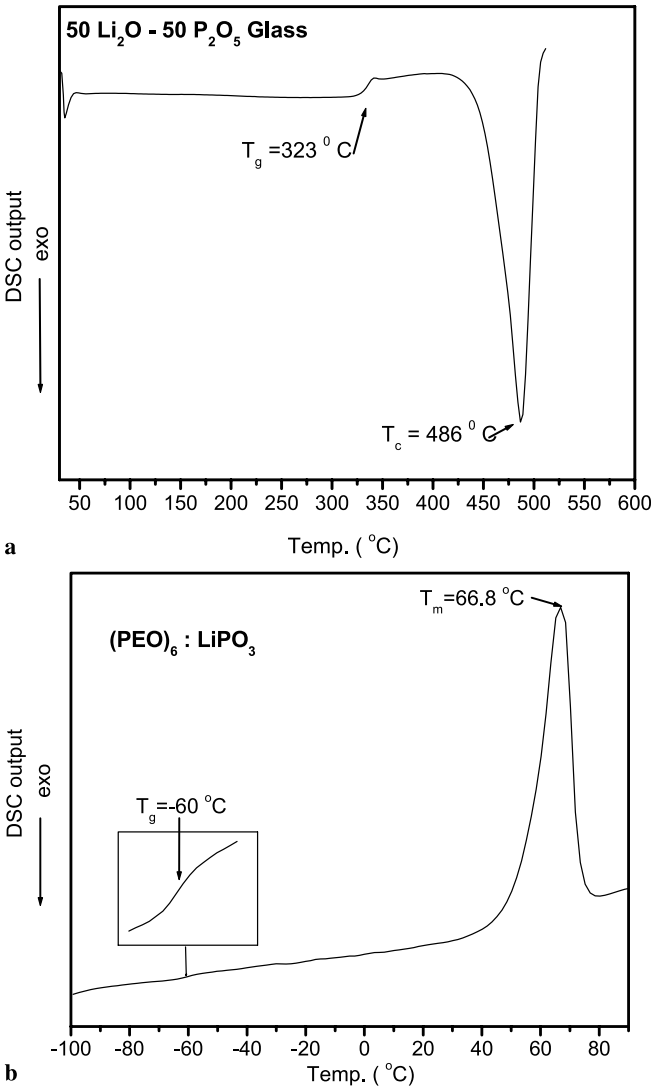

FIGURE 2 (**a**) DSC curve of Li_2O-P_2O_5 glass; (**b**) DSC curve of $(PEO)_6$: $LiPO_3$

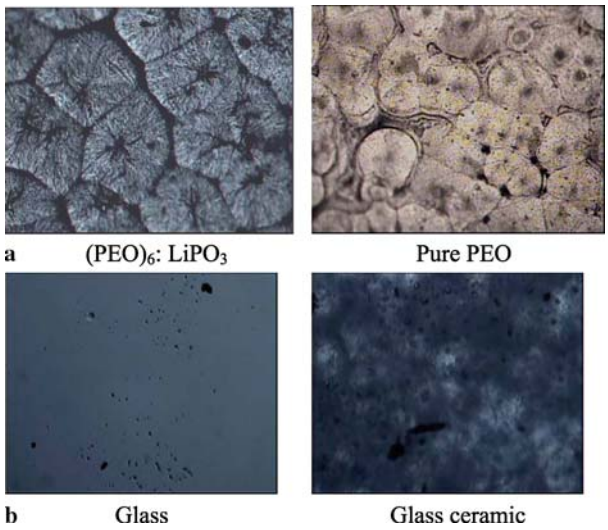

FIGURE 3 (**a**) Optical micrographs of (i) $(PEO)_6$: $LiPO_3$ and (ii) PEO; (**b**) Optical micrographs of Li_2O-P_2O_5 glass and $LiPO_3$ glass-ceramic

was low, probably due to the residual glassy matrix in the glass-ceramic.

Pure PEO exhibits a semi-crystalline nature with two prominent peaks around 19° and 24°. $(PEO)_6$: $LiPO_3$ metal salt complex has been characterized based on the broadening of the above XRD peaks of PEO along with a reduction in the intensity of the peaks. This observation confirms the complex formation of crystalline $LiPO_3$ with PEO polymer. It also indicates to the fact that there is an increase in the amorphous phase of the system due to complexation, which is of critical importance from the point of view of enhancement in the conductivity of the complex phase. The presence of low intense diffraction peaks corresponding to the strong lines of $LiPO_3$ salt can be attributed to the presence of traces of uncomplexed salt.

The DSC spectrum for mol % $50Li_2O$-$50P_2O_5$ glass in the temperature range of 30–500 °C is shown in Fig. 2a. The glass transition temperature (T_g) is seen as a small endothermic hump around 323 °C. With further heating, the glass gets devitrified exhibiting a sharp exothermic peak around 486 °C known as crystallization temperature (T_c).

The DSC plot, (Fig. 2b), for $(PEO)_6$: $LiPO_3$ shows T_g at −60 °C where the polymer undergoes a transition from brittle and hard nature to a soft, flexible amorphous nature which is an endothermic process (for pure PEO, $T_g = -68$ °C). On further heating, another endothermic peak corresponding to the melting of the crystalline phase of the polymer-metal salt complex is observed at $T_m = 66.8$ °C (for pure PEO, $T_m = 68$ °C). Thus with the addition of the salt, the DSC spectrum shows a shift in T_g and T_m values. The increase in the T_g value is due to the polymer-metal salt complexation, with the formation of a co-ordinate bond between the ether-oxygen of the polymer and the cation of the salt. As a result of this, the host polymer matrix gets stiffened and hence, T_g increases from −68 °C to −60 °C. The degree of crystallinity of the polymer metal salt complex can be calculated by considering the enthalpy of melting, i.e., the area under the melting peak at 64 °C. The percentage degree of crystallinity $\%X_c$ is given by

$$\%X_c = (\Delta H/\Delta H_0) \times 100\,, \tag{2}$$

where ΔH is the enthalpy of melting of polymer metal salt complex and ΔH_0 (213.7 J/g) is the enthalpy of melting of 100% crystalline PEO [10, 11]. The percentage of crystallinity of host polymer (PEO) gets reduced from 62.6% to 42.7% on complexation with $LiPO_3$. The reduction in the crystallinity on addition of salt is attributed to the strong interaction of metal salt with the host polymer.

An optical micrograph of the $(PEO)_6$: $LiPO_3$ metal salt complex in Fig. 3a exhibits a complete spherulitic texture with "eye like" morphology near the spherulitic center. The micrograph of the pure PEO film shows bright and dark regions in the form of stripes which corresponds to the crystalline and amorphous phase of the polymer. With the addition of the salt, the dark region corresponding to the amorphous phase increases, indicating enhancement in the amorphous rich phase and, additionally, uniformly arranged spherulitic nuclei like structure are observed. The above microstructural observation is in agreement with XRD and DSC results which have indicated an enhancement in the amorphous phase.

The complex impedance plots of all the phases have been shown in Fig. 4. The ionic conductivity of polycrystalline $LiPO_3$ is low with $\sigma_{dc} = 2.5 \times 10^{-8}\,Scm^{-1}$ at 280 °C (Fig. 4a) due to the absence of open structure and presence of grain boundaries [12]. In polycrystalline $LiPO_3$, lithium ion conduction takes place through an interstitial mechanism as shown in Fig. 5. In $LiPO_3$ crystal, the corner sharing PO_4 groups form chains. In each PO_4 unit, two of the oxygen atoms take part in bridging the neighboring PO_4 group and the remaining two are non-bridging oxygen (NBO) atoms. The Li atoms lie between the PO_3 chain and the NBO atoms of PO_4 group form tetrahedral coordination around each Li atom. The short P–O bond length between the central phosphorus and the NBOs is in the range of 1.45–1.52 Å. The long P–O distances between P and bridging oxygen atoms occur in the range 1.57–1.63 Å [3]. The ions migrate through edge-shared distorted interstitial tetrahedral sites with an activation energy of 1.4 eV.

Glass sample mol % $50Li_2O$-$50P_2O_5$ exhibits ionic conductivity value of $\sigma_{dc} = 4.5 \times 10^{-4}\,Scm^{-1}$ at 280 °C, which is four orders higher than that of polycrystalline $LiPO_3$ (Fig. 4b). As shown in the inset of Fig. 4b, the logarithm of conductivity is found to be inversely proportional to the absolute temperature, obeying the Arrhenius relation [13]. Absence of long-range order and availability of open structure for ion migration are attributed to the high ionic conductivity of the glass with a low activation energy of 0.76 eV, which is half that of Li^+ ion motion in its polycrystalline counterpart. The structure of phosphate glass is formed by PO_4 tetrahedra connected by corners. Vitreous P_2O_5 has a 3-D network build up with PO_4 tetrahedra, connected by three of their four corners (Q^3). The fourth one is occupied by terminal double bonded oxygen. Introducing the glass modifier Li_2O results in depolymerization of the phosphate crosslinked network with the breaking of P–O–P bonds and the formation of non-bridging oxygens, i.e. Q^3 to Q^2 (in Q^n terminology, n denotes the number of P–O–P bonds in PO_4 tetrahedra [14]). In the present investigation on mol % $50Li_2O$-$50P_2O_5$ glass, the long tetrahedra PO_4 chain is depolymerized to rather short chains [15, 16]. The Li atoms are coordinated by the non-bridging oxygen atoms of these randomly oriented phosphate chains. Based on the above literature as well as the experimental results, the

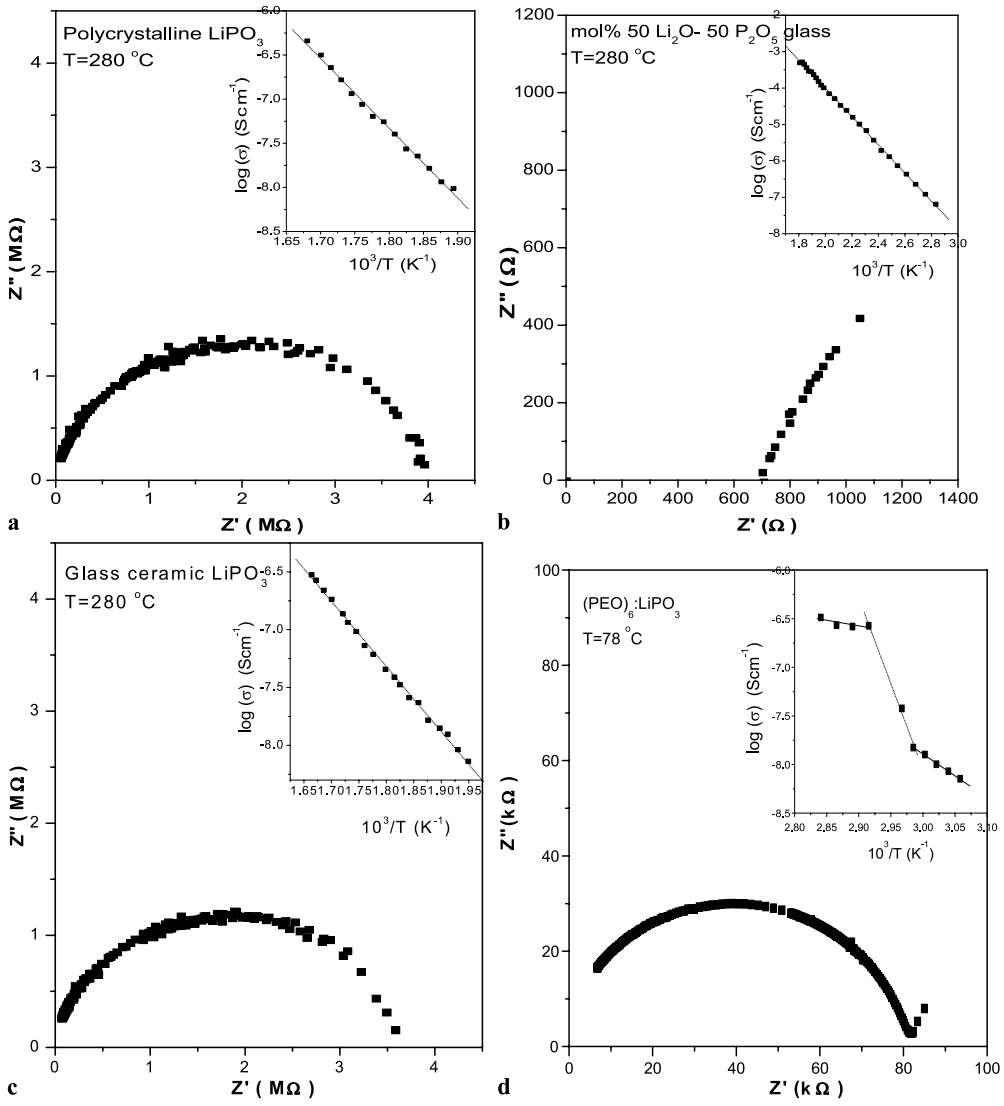

FIGURE 4 Impedance plots of (**a**) $LiPO_3$ polycrystalline; (**b**) Li_2O-P_2O_5 glass; (**c**) $LiPO_3$ glass-ceramic and (**d**) $(PEO)_6$: $LiPO_3$. *Inset*: Temperature variation of conductivity

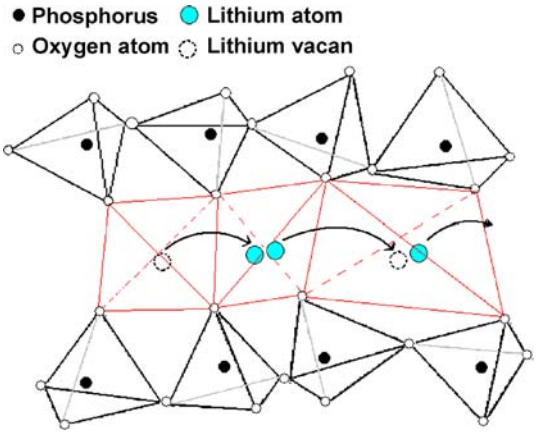

FIGURE 5 Schematic representation of ion migration in polycrystalline $LiPO_3$

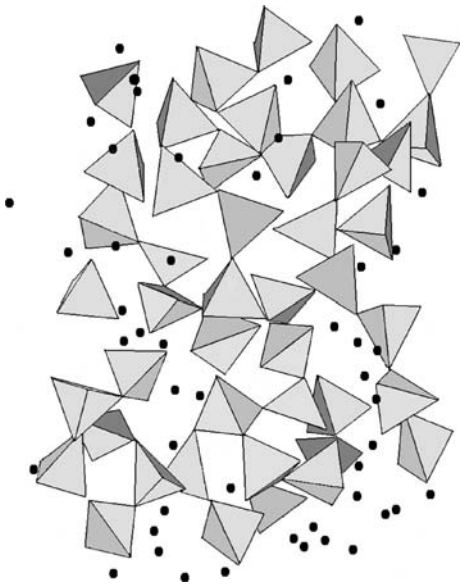

FIGURE 6 Schematic representation of Li_2O-P_2O_5 glass network with random distribution of Li^+ ions. *Dark circles* refer to Li^+ ions and *tetrahedra* represent PO_4 groups

random distribution of Li^+ ions in the chosen glass network is schematically shown in Fig. 6. Simulation studies by reverse Monte Carlo modeling and valence bond analysis identify the pathways for Li^+ ion motion [17, 18]. The mechanism for fast ion transport in the glass may result from the hopping of mobile ions between various vacant sites through these pathways. Thermodynamic modelling approaches to phosphate glasses such as Ag_2O-P_2O_5 and Na_2O-P_2O_5 suggests that this mode of ion migration occurs through the "interstitial pair formation" mechanism [19–21]. However, the mechanism of these hopping motions is complex and several coexisting models such as strong electrolyte [22], weak electrolyte [23], random site model [24] and cluster bypass model [25] have been proposed to explain the transport process.

Glass-ceramic has the same XRD characteristics as polycrystalline $LiPO_3$ but with different microstructure, exhibiting a better conductivity value of $\sigma_{dc} = 4.2 \times 10^{-8}\,Scm^{-1}$ at 280 °C (Fig. 4c). The phase morphology was investigated through optical microscopy. Figure 3b represents the evolution of glass to glass-ceramic transition, when the glass is subjected to controlled heat treatment. On annealing the glass sample above its T_g, at 380 °C, devitrified crystallites were formed and uniformly dispersed in the glass. On further annealing, crystalline domains appear as dark areas. The micrograph reveals a dark interconnected network of crystallites with a translucent residual glassy matrix. The absence of pores and the presence of a residual glassy phase in the glass-ceramic slightly enhanced the conductivity when compared to that of the polycrystalline phase. Furthermore, the activation energy for ionic conduction, ($E_a = 1.2$ eV), is lower than that of polycrystalline $LiPO_3$.

Figure 4d (inset) shows the temperature variation of the conductivity of $(PEO)_6$: $LiPO_3$ complex. The above variation in conductivity can be discussed on the basis of the presence of two phases, i.e., amorphous and crystalline phase of the polymer salt complex. PEO has a helical structure with a 19.3 Å repeat unit consisting of seven CH_2CH_2O units in two turns of the helix, having CCOC and OCCO atoms predominantly in trans (∼180°) and gauche (±60°) conformation, respectively. Due to the influence of conformation, there is a considerable distortion in the helical symmetry of PEO, indicating a high degree of flexibility. In general, the CCOC's trans conformation is practically independent of salt concentration. However, the addition of salt shows marked increase in gauche (±60°) population [7, 26]. Generally, a complex like $(PEO)_6$: $LiPO_3$ is formed such that the lithium ions are coordinated along the axis of the polymer helical chain. Here the oxygen atoms act as donors for the cation (Li^+) while anion (PO_3^-), generally of large dimension, stabilizes the $(PEO)_6$: $LiPO_3$ complex [27–30]. The schematic representation of ether-oxygen and the cation is illustrated in the Fig. 7. At temperatures below T_m, the Li^+ ion migrates from one site to another within the oxygen-lined tunnels by making and breaking co-ordinate bonds with oxygen of PEO (Fig. 7a). This type of ionic motion in a $(PEO)_6$: $LiPO_3$ system, with an enhanced amorphous phase as revealed through DSC, accounts for the Arrhenius type of conductivity behavior below T_m [31]. At T_m, the whole system becomes amorphous, thus, the conductivity jumps to higher values. Above T_m, the formerly crystalline part of the complex mixes with the formerly amorphous parts, leading to an equilibration of the lithium salt concentration in the whole system. Here, mainly the segmental motion of the polymer, in addition to hopping motion within the oxygen lined tunnels, is thought to promote ion motion in a dynamically disordered environment by providing space into which the ion may diffuse under the influence of an electric field (Fig. 7b). Each PEO chain extends to approximately four or five turns, since the likelihood of extended regular helices in amorphous phases is quite low. Each chain is separated from the next chain by an amorphous region. Ion motion within the oxygen lined tunnel is followed by motion via bridging sites in the amorphous regions before the cation enters the next helix. For amorphous polymer electrolyte, where both ionic mobility and segmental motion of polymer host contribute to ionic conduction, the observed temperature dependence of the conductivity can be fitted to the empirical Vogel–Tammann–Fulcher (VTF) relation [32]. However, in the present case, a linear plot in $\log \sigma$ versus $10^3/T$ has been

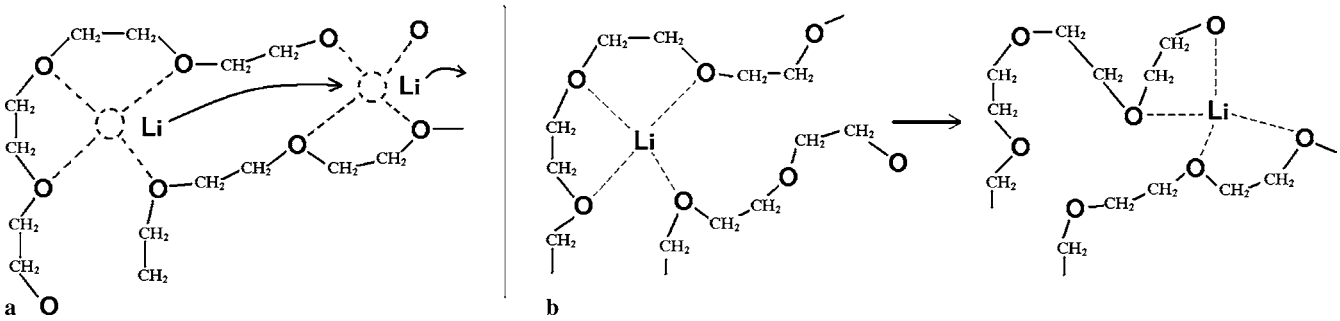

FIGURE 7 Schematic representation of conduction by (**a**) hopping and (**b**) segmental motion in $(PEO)_6$: $LiPO_3$

observed below and above the softening point, which could be fitted to Arrhenius relation. Similar conductivity behavior has been reported in a number of PEO based polymer electrolytes [33, 36]. Thus, the newly identified $(PEO)_6$: $LiPO_3$ system exhibits an ionic conductivity of 3.1×10^{-7} Scm^{-1} at 78 °C, with activation energies of 0.88 eV and 0.21 eV, below and above the softening point, respectively.

4 Conclusion

$LiPO_3$, a simple and unique material, has enabled the investigation of Li^+ ion conduction characteristics in different phases, namely, polycrystalline $LiPO_3$, Li_2O-P_2O_5 glass and $LiPO_3$ glass-ceramic (devitrified glass). It is to be noted that the best Li^+ ion conduction has been observed in glassy networks, followed by glass-ceramic and crystalline phases. Furthermore, a new polymer-metal salt complex has been realized with good conduction characteristics at relatively low temperature.

REFERENCES

1 M. Vogel, Phys. Rev. B **68**, 184 301 (2003)
2 M. Vogel, Phys. Rev. B **70**, 094 302 (2004)
3 K. Muruganandam, M. Seshasayee, S. Patnaik, Solid State Ionics **89**, 313 (1996)
4 T.M. Alam, J.J. Liang, R.T. Cygan, Phys. Chem. Chem. Phys. **2**, 4427 (2000)
5 A. Triolo, V. Arrighi, R. Triolo, S. Passerini, M. Mastragostino, R.E. Lechner, R. Ferguson, O. Borodin, G.D. Smith, Physica B **301**, 163 (2001)
6 M.J.C. Plancha, C.M. Rangel, C.A.C. Sequeira, Portugaliae Electrochimica Acta **15**, 121 (1997)
7 M. Armand, Solid State Ionics **69**, 309 (1994)
8 C.A. Vincent, Prog. Solid. State. Chem. **17**, 145 (1987)
9 P.J.C. Guitel, I. Tordjman, Acta Cryst. B **32**, 2960 (1976)
10 J.H. Shin, K.W. Kim, H.J. Ahn, J.H. Ahn, Mater. Sci. Eng. B **95**, 148 (2002)
11 X. Jingyo, X. Tang, Electrochim. Acta **51**, 4765 (2006)
12 M. Pouchard, P. Hagenmuller, *Solid Electrolyte*, ed. by P. Hagenmuller, W. Van Gool (Academic Press, New York, 1978) pp. 199
13 S.W. Martin, C.A. Angell, J. Non-Cryst. Solids **83**, 185 (1986)
14 E. Lippma, M. Magi, A. Samoson, G. Englehardt, A.R. Grimmer, J. Am. Chem. Soc. **102**, 4889 (1980)
15 J.J. Liang, R.T. Cygan, T.M. Alam, J. Non-Cryst. Solids **263–264**, 167 (2000)
16 R.K. Sistla, M. Seshasayee, J. Non-Cryst. Solids **349**, 22 (2004)
17 S. Adams, J. Power Source. **159**, 200 (2006)
18 S. Adams, Bull. Mater. Sci. **29**, 587 (2006)
19 D. Coppo, M.J. Duclot, J.L. Souquet, Solid State Ionics **90**, 111 (1996)
20 J.L. Soquet, M. Duclot, M. Levy, Solid State Ionics **105**, 237 (1998)
21 G.D.L.K. Jayasinghe, P.W.S.K. Bandaranayake, J.L. Soquet, Solid State Ionics **86–88**, 447 (1996)
22 O.L. Anderson, D.A. Stuart, J. Am. Ceram. Soc. **37**, 573 (1954)
23 D. Ravaine, J.L. Soquet, Phys. Chem. Glass. **18**, 27 (1977)
24 A.M. Glass, K. Nassau, J. Appl. Phys. **51**, 3756 (1980)
25 M.D. Ingram, M.A. Mackenzie, W. Muller, M. Torge, Solid State Ionics **28–30**, 677 (1988)
26 B.A. Ferreira, F. Müller-Plathe, A.T. Bernardes, W.B. De Almeida, Solid State Ionics **147**, 361 (2002)
27 Y.G. Andreev, P.G. Bruce, Electrochim. Acta **45**, 1417 (2000)
28 D. Brandell, A. Liivat, H. Kasemagi, A. Aabloo, J.O. Thomas, J. Mater. Chem. **15**, 1422 (2005)
29 G.S. Mc Glashan, Y.G. Andreev, P.G. Bruce, Nature **398**, 792 (1999)
30 Y.G. Andreev, V. Seneviratne, M. Khan, W.A. Henderson, R.E. Frech, P.G. Bruce, Chem. Mater. **17**, 767 (2005)
31 P.V. Wright, Brit. Polym. J. **7**, 319 (1975)
32 M.A. Ratner, *Polymer Electrolyte Rev. 1*, ed. by J.R. MacCallum, C.A. Vincent (Elsiever Applied Science Publishers, London, New York, 1987) pp. 173
33 D. Golodnitsky, G. Ardel, E. Peled, Solid State Ionics **147**, 141 (2002)
34 M.B. Armand, *Polymer Electrolyte Rev. 1*, ed. by J.R. MacCallum, C.A. Vincent, (Elsiever Applied Science Publishers, London, New York, 1987) pp. 8
35 D. Golodnitsky, G. Ardel, E. Strauss, E. Peled, Y. Lareah, Y. Rosenberg, J. Electrochem. Soc. **144**, 3484 (1997)
36 F. Huguenin, M.G. Cavalcante, R.M. Torresi, Solid State Ionics **126**, 259 (1999)